Int. J. Electrochem. Sci., 11 **(2016)** 9687 – 9695, doi: 10.20964/2016.11.49

International Journal of
ELECTROCHEMICAL
SCIENCE
www.electrochemsci.org

Investigation of CA/G/MnO_2 Electrode Composite for Supercapacitors

Liquan Lu[1,*], *Shengming Xu*[2], *Junwei An*[2]

[1] School of Mechatronics Engineering, North University of China, Taiyuan 030051, China
[2] Institute of Nuclear and New Energy Technology, Tsinghua University, Beijing 100084, China
[*]E-mail: lq_lu@buaa.edu.cn

Received: 12 August 2016 / *Accepted:* 22 September 2016 / *Published:* 10 October 2016

In this paper, we have successfully synthesized a cellulose acetate/graphene/MnO_2 (CA/G/MnO_2) composite, which is further employed as an electrode material for supercapacitors. This novel composite material can fully utilize the conductivity of the graphene and the dense internal structure of the cellulose acetate (CA) to increase the specific capacitance of the MnO_2. At the current density of 0.1 A/g, the specific capacitance of the CA/G/MnO_2 composite is 1181 F/g, which is very close to the theoretical capacitance. Moreover, the capacitance of the CA/G/MnO_2 composite finally stabilizes at 93 F/g, after 5000 cycle charge and discharge test under the high current density of 30 A/g. Its capacitance retention rate is 67.4%, which is great higher that the capacitance retention rate of the MnO_2 (44.2%). These results fully indicate that the CA/G/MnO_2 composite has broad application prospects in the field of super capacitor electrode materials.

Keywords: Supercapacitors; Cellulose acetate; Graphene; Electrode materials

1. INTRODUCTION

As a kind of pseudo capacitor material, MnO_2 has the characteristics of low price, environment friendly, and relatively high theoretical capacitance (~1200 F/g), which has a very broad application prospects in the field of super capacitor [1-6]. In recent years, the research that MnO_2 is employed as super capacitor electrode materials mainly focuses on the preparation, characterization and performance characterization of the nano MnO_2 particles [5-9]. It is reported by Zhu et al. that a MnO_2 nano flowers synthesized by a hydrothermal method has high capacitance, as well as good cycle stability [7]. To promote the physical properties and electrochemical properties of MnO_2, considerable efforts have been made on the synthesis of the composite electrode materials with high specific capacitance and good loop stability [7-9]. Studies show that some of the carbon materials with good

conductivity, such as: carbon nanotubes (CNTs), graphene [10] and carbon black, etc., compositing with pseudo capacitance materials can enhance the conductivity and loop stability of the material [7-9,11]. The specific capacitance of a composite electrode material, composed by carbon nanotubes, graphene and MnO_2, reaches to 319 F/g in 1 M $NaSO_4$ solution at the current density of 0.5 A/g [8]. In order to enhance the specific capacitance of the materials, the researchers try to obtain MnO_2 fibers grown on some array carbon materials and oxides [11-16]. Acetate fibers with smooth surface and compact structure have the characteristics of large-scale industrial preparation, so it has potential application value in improving the material specific capacitance. [17]

In this paper, the MnO_2 nonofibers are in situ grown on the surface of the CA/G carrier to form a cellulose acetate/graphene/MnO_2 (CA/G/MnO_2) composite, in which the MnO_2 nonofibers successfully is closely combined with the graphene with good conductivity. The results indicate that, the CA/G/MnO_2 composite has higher specific capacitance and better cycle stability, compared to the MnO_2.

2. EXPERIMENTAL

2.1 Synthesis of the graphene

The graphene oxide is prepared by a modified Hummers method [18,19]. In brief, 50 g expandable graphite and 25 g sodium nitrate are mixed with 500 ml concentrated sulfuric acid in a 2 l beaker, which is put in a water bath fixed at 0 ºC. Subsequently, 300 g potassium permanganate is added into the mixture in 6 times under gently stirring in 1 h. Then, the temperature of the mixture is hold at 35 ºC for 30 min. After 920 ml distilled water is slowly added into the beaker, the mixture is stirred for 1 h and aged for 12 h, successively. After maintained at 98 ºC for 1 h, the mixture is filtrated. A graphene oxide can be obtained, after the filter residue is dried and annealed at 350 at Ar atmosphere.

Thereafter, 0.65 g graphene oxide is dispersed in 0.5 l acetic acid in a flask by ultrasonic agitation for 30 min. Then the flask is placed in a water bath fixed at 40 °C. After 15 ml hydriodic acid is added to the flask, the reaction mixture is incubated for 40 h at 40 °C. After neutralized using saturated sodium bicarbonate solution, the mixture is filtrated. Finally, the reduced graphene is obtained, after the filter residue is washed and dried in a vacuum oven for 12 h at 80 °C.

2.1 Preparation of the CA/G/MnO_2 composite

The preparation processes of the CA/G/MnO_2 composite are as follows: firstly, 0.5 g fragmented cellulose acetate membrane (purchased from Sinopharm Chemical Reagent Co., Ltd, China) is dissolve in 30 ml acetone, using mechanical agitation. Then, 0.1 g graphene is added into the mixture, by high speed stirring for 10 min and ultrasonic agitation for 20 min. Subsequently, the flask containing the solution is put in the water bath hold at 80 °C, until the solution is evaporated. At room temperature, the above mixture is again dispersed in 150 ml ethanol by ultrasonic agitation for 15 min.

After the mixture is filtrated, the filter residue (CA/G composite) is washed and dried in a vacuum oven for 2 h at 80 °C. Thereafter, 0.06 g CA/G composite is mixed with 20 ml 0.05 M manganous acetate solution and 7 ml ethanol in a flask by high speed stirring for 10 min. Then, the flask is placed in a water bath maintained 60 °C. After the solution is evaporated, 200 ml 0.02 M potassium permanganate solution is added into the flask. Then, the reaction mixture is hold at 80 °C for 20 h. After the mixture is filtrated, the filter residue is washed by ethanol adequately. Finally, the CA/G/MnO_2 composite is obtained, after the filter residue is dried in a vacuum oven for 5 h at 80 °C. For comparison, the pure MnO_2 is prepared by same method without adding any support materials.

2.3 Characterization of electrode materials

The morphologies of acetate fiber and graphene are investigated using a Tecnai G2 F20 S-TWIN transmission electron microscope (TEM, FEI). The acetate fiber sample is fabricated by dropping the dispersion of the cellulose acetate, prepared by dissolving 1 mg of the cellulose acetate membrane in 2 ml acetone, on a copper grid coated with amorphous carbon film, dried in air at room temperature. The morphologies of CA/G/MnO_2 composites before and after electrochemical measurement are observed by a HITACHI S-4800 scanning electron microscope (SEM). The X-ray powder diffraction data of the acetate fiber, graphene, pure MnO_2 and CA/G/MnO_2 composite are collected using a Rigaku Dmax 2400 X-ray diffractometer.

2.4 Electrochemical test

The electrochemical performance of the electrode materials is investigated using a CHI 760E electrochemical workstation (Shanghai, China) by a three electrodes system. The electrolyte solution 2 M Na_2SO_4 solution, whose pH is adjusted to 10 by KOH solution. The working electrode is manufactured based on the method described in literature [19-22]. Briefly, 20 μl composite ink, prepared by mixing 20 mg electrode material, 4 ml ethanol and 30 μl Nafion solution (5 wt%, DuPont Corp,. USA), is placed on a polished glassy carbon working electrode (Φ = 5 mm) using a microsyringe. An Ag|AgCl electrode and a sheet of platinum (2 cm^2) are respectively employed as the reference electrode and counter electrode.

3. RESULTS AND DISCUSSION

3.1 Electrode materials characterization

Figure 1 indicates the morphologies of the acetate fiber, graphene and CA/G/MnO_2 composites. As can be seen from the TEM image of the acetate fiber (Figure 1a), it has smooth surface morphology [17]. Figure 1b is the TEM image of the graphene, which shows that the surface of the graphene contains a large amount of folding under the action of the surface free energy, because the overlap between graphene layers or the transformation from the two-dimensional (2D) to 3D of graphene with few layers can decrease the surface energy [19,23,24]. The folding of the graphene makes the specific

surface area of the graphene decrease slightly. Figure 1c and d respectively are the SEM images of the CA/G/MnO_2 composites before and after electrochemical test (charge-discharge test at the current density of 30 A/g for 5000 circles). Figure 1c indicates that the CA/G/MnO_2 composite exhibits perfect honeycomb structure. Moreover, it was difficult to discover separate acetate fiber and graphene in Figure 1c. These results suggest that the cellulose acetate, graphene and MnO_2 nanofibers are organically combined in the CA/G/MnO_2 composite, implying that the interior of the CA/G/MnO_2 composite is filled with the network structure constructed by the cellulose acetate and graphene. This structure can effectively maximize the advantages of the graphene to improve the transfer of Faraday charge in the CA/G/MnO_2 composite. Furthermore, the honeycomb structure of the CA/G/MnO_2 composite makes the MnO_2 nonofibers are fully contacted with the electrolyte solution, which profits to improve the capacitance and the cycle stability of the CA/G/MnO_2 composite. The SEM image of the CA/G/MnO_2 composite after electrochemical test is shown in Figure 1d, which reveals that partial honeycomb structure are still retained in the CA/G/MnO_2 composite, suggesting that the unique honeycomb structure can effectively prevent the accumulation of the composite material. The good stability of the honeycomb structure is advantageous to strengthening the cycle stability of the CA/G/MnO_2 composite.

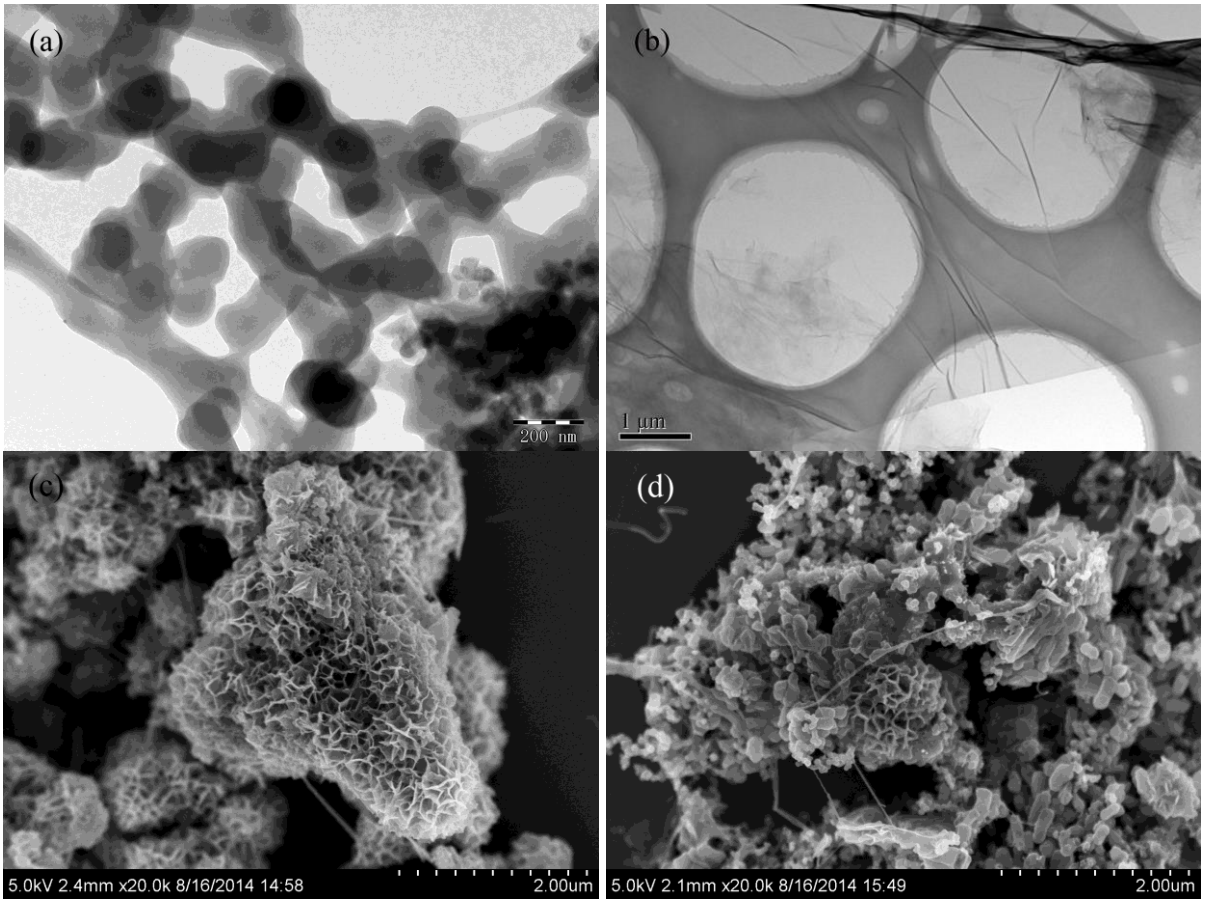

Figure 1. TEM images of the acetate fiber (a) and graphene (b), SEM images of the CA/G/MnO_2 composites before (c) and after (d) electrochemical test.

The XRD patterns of the graphene, acetate fiber, pure MnO_2 and CA/G/MnO_2 composite are displayed in Figure 2. A wide diffraction peak of the graphene appears at 2θ = 22°, which is less than that (2θ = 26°) of the graphite (JCPDS No. 25-284). The reason is that the thickness of graphene is thinner than that of graphite, resulting in the diffraction angle shift to low degree. Therefore, the wide diffraction peak at of the graphene suggests that there are large differences among the thicknesses of the prepared graphene, due to the incomplete separation of the graphite sheets, or the accumulation of the graphene sheets. Moreover, the typical diffraction peak of the graphene oxide (2θ = 10°) does not appear in the XRD pattern of the graphene, which implying that the graphene oxide hardly exist in the prepared graphene. The wide peak of the acetate fiber is located at 2θ = 19°, suggesting that its crystallinity is not high. As can be seen from Figure 2, the typical diffraction peaks (2θ = 12°, 25.7°, 36.8°and 66°) of the MnO_2 (JCPDS No. 18-0802) are appeared in the XRD patterns of the pure MnO_2 and CA/G/MnO_2 composite, indicating again that the MnO_2 nonofibers are successfully combined with the cellulose acetate and graphene.

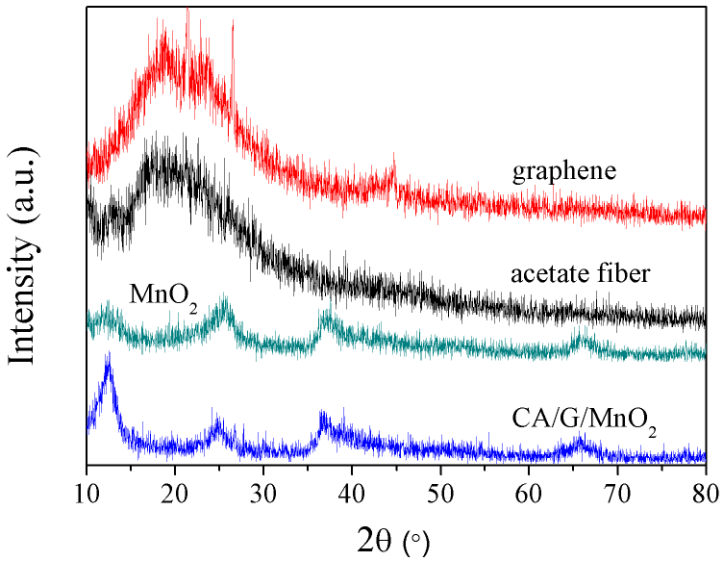

Figure 2. XRD patterns of the graphene, acetate fiber, pure MnO_2 and CA/G/MnO_2 composite.

3.2 Electrochemical test

Figure 3 exhibits the CVs of the CA/G/MnO_2 composite and MnO_2. The CVs of the CA/G/MnO_2 composite at different scanning rates are displayed in Figure 3a, which shows that the CVs of the CA/G/MnO_2 composite at low scanning rates maintain a rectangle shape; while the rectangle shape of the CVs gradually deforms with the increase in the scanning rate, especially at the high scanning rate of 200 mV/s. The rectangle shape of its CV at low scanning rate (2mV/s) illustrates the good capacitive performance of the CA/G/MnO_2 composite. The deformed rectangle shape of the CVs at high scanning rates suggests that the capacitance performance of the CA/G/MnO_2 composite is weakened, due to the capacitive decay under high scanning rates [25]. Figure 3b compares the CVs of the CA/G/MnO_2 composite and pure MnO_2 at 200 mV/s, which indicates that the area of the

rectangular CV of the CA/G/MnO_2 composite is larger than that of the pure MnO_2, showing that the addition of cellulose acetate and graphene greatly improves the capacitance of the pure MnO_2 [25,26].

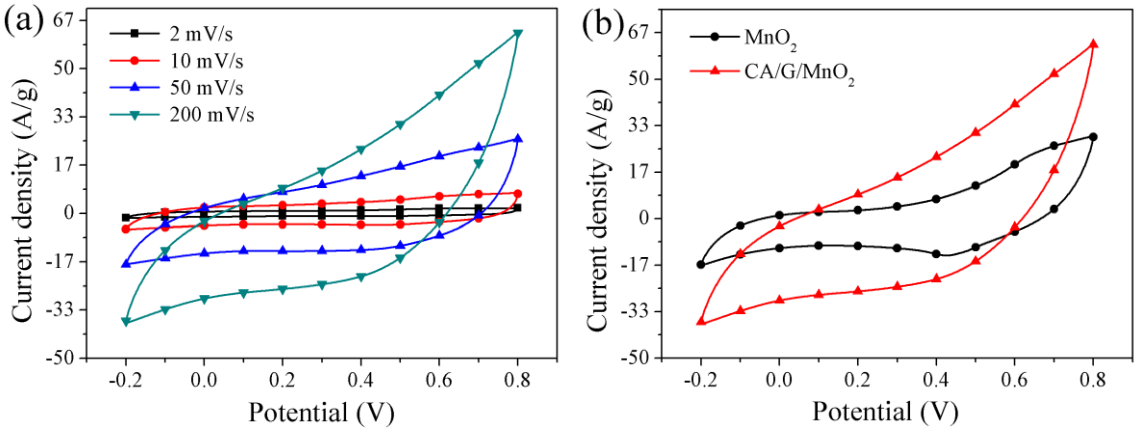

Figure 3. (a) CVs of the CA/G/MnO_2 composite at different scanning rates; (b) CVs of the CA/G/MnO_2 composite and MnO2 nonofibers at the scanning rate of 200 mV/s.

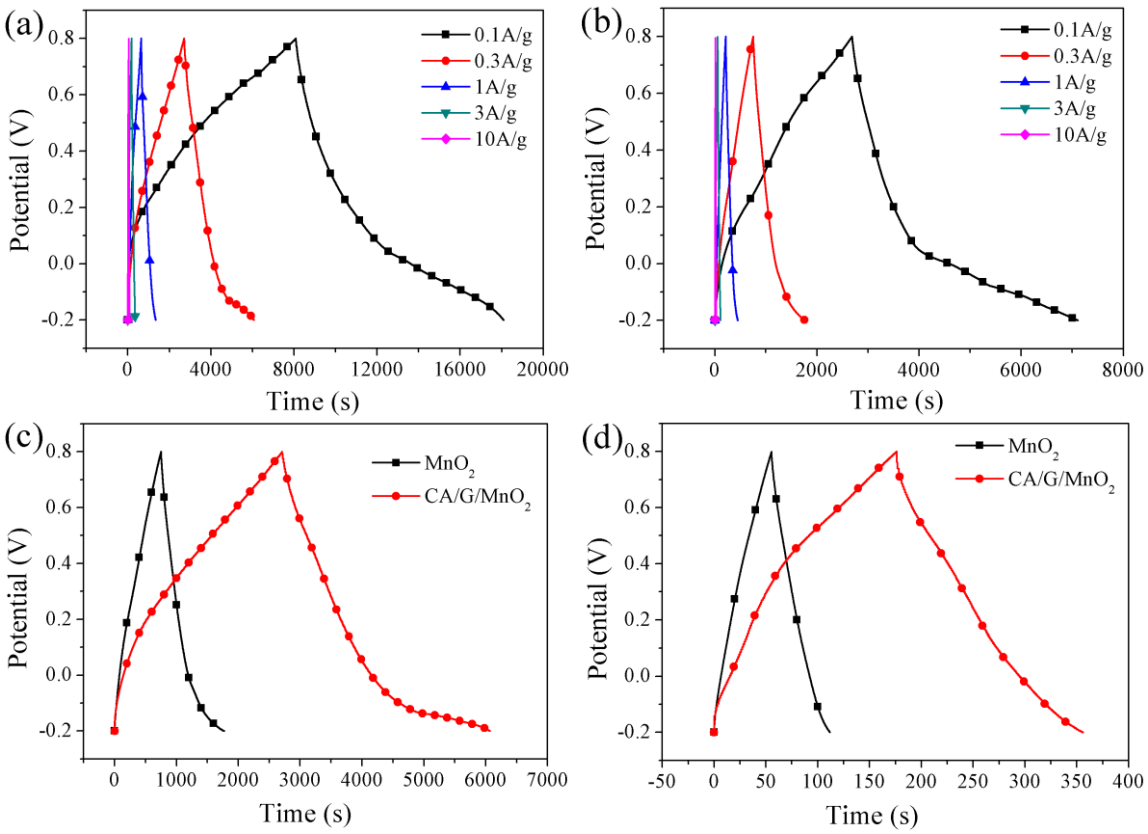

Figure 4. (a) GCD curves of the CA/G/MnO_2 composite at different current densities; (b) GCD curves of pure MnO_2 at different current densities; (c) GCD curves of the CA/G/MnO_2 composite and at MnO_2 at the current density of 0.3 A/g; (d) GCD curves of the CA/G/MnO_2 composite and at MnO_2 at the current density of 3 A/g.

The reason that the CA/G/MnO_2 composite has high capacitance is associated with its unique honeycomb structure, which makes the smooth dense fibrous structure of the cellulose acetate and the high conductivity of the graphene are fully utilized to improve the capacitance of the MnO_2. Furthermore, the CV curve of the MnO_2 in Figure 3b shows a pair current peaks at the potential range of 0.4-0.7 V, which is associated with the Faradaic redox reaction [27,28]. However, none of the redox peaks appears in the CV curves of the CA/G/MnO_2 composite at all the scan rate, implying its good electrochemical reversibility [29-31].

The galvanostatic charge–discharge (GCD) curves of the CA/G/MnO_2 composite and MnO_2 are revealed in Figure 4. The GCD curves of the CA/G/MnO_2 composite and MnO_2 at different current densities are shown in Figure 1a and b, respectively. As can be seen from Figure 1a and b, the specific capacitances of the CA/G/MnO_2 composite and MnO_2 decrease with increasing current densities, because the electrode materials cannot fully contact with the electrolyte solution. According to Figure 1a and b, the calculated specific capacitance of the CA/G/MnO_2 composite at the current densities of 0.3 and 0.1 A/g are respectively 1155 and 1181 F/g, which are 3.7 and 2.6 times higher than those pure MnO_2 fiber at 0.3 (306 F/g) and 0.1 A/g (443F/g) [32]. Moreover, the specific capacitance of the CA/G/MnO_2 composite is higher than that of the reported MnO_2 electrode materials [5,6]. Figure 4c and d compares the GCD curves of the CA/G/MnO_2 composite and MnO_2 respectively at the current density of 0.3 and 3 A/g. It can be seen clearly from Figure 4c and d that the specific capacitances of the CA/G/MnO_2 composite are higher than those of the MnO_2 at the current densities of 0.3 and 3 A/g. These results again prove that the addition of cellulose acetate and graphene significantly improves the capacitance of the pure MnO_2. This conclusion is consistent with the result of the CV test.

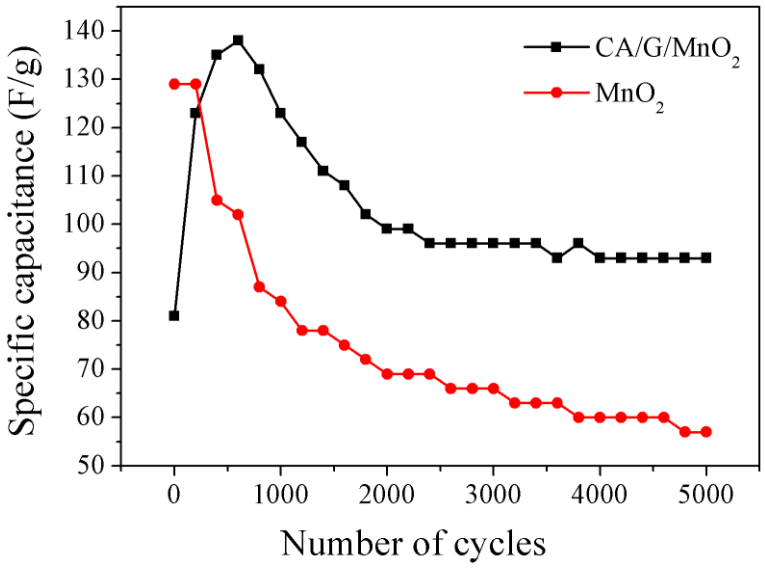

Figure 5. Charge-discharge cycle curves of the CA/G/MnO_2 composite and MnO_2 at the current density of 30 A/g for 5000 circles.

The charge-discharge cycle curves of the CA/G/MnO_2 composite and MnO_2 at the current density of 30 A/g for 5000 circles is displayed in Figure 5, which presents that the specific capacitance

of the CA/G/MnO_2 composite after charge-discharged for 5000 laps at the current density of 30 A/g is stabilized at 93 F/g, its capacitance retention rate reaches to 67.4%. However, the specific capacitance of the pure MnO_2 after 5000 laps at 30 A/g is only 57 F/g, and the corresponding capacitance retention rate is about 44.2%. Furthermore, the cycle stability of the CA/G/MnO_2 composite is better the reported MnO_2 electrode materials [5,6]. These results suggest that the addition of cellulose acetate and graphene not only greatly improves the capacitance of the pure MnO_2, but also markedly enhances the cycle stability of the pure MnO_2. The reason is related to the unique honeycomb structure of the CA/G/MnO_2 composite, which effectively prevents the electrode material from being accumulated.

4. CONCLUSION

Adopting a simple method, the MnO_2 nanofibers are grown in situ on the surface of the acetate fiber and graphene to synthesize the CA/G/MnO_2 composite, with the aim of improving the capacitance, conductivity and cycling stability of the MnO_2. The CA/G/MnO_2 composite is successfully investigated as a supercapacitor electrode material. The results indicate that the cellulose acetate, graphene and MnO2 nonofibers are organically combined in the CA/G/MnO_2 composite to form a perfect honeycomb structure. The good stability of the CA/G/MnO_2 composite with honeycomb structure and excellent coordination among the graphene, cellulose acetate and MnO_2 nanofibers make the CA/G/MnO_2 composite has high capacitance and wonderful cycle stability, simultaneously. The electrochemical test result indicate that the capacitance of the CA/G/MnO_2 composite at the current densities of 0.3 and 0.1 A/g are respectively 1155 and 1181 F/g, which is very close to the theoretical capacitance of the MnO_2 (1200 F/g). Moreover, the capacitance retention rate is 67.4% of the CA/G/MnO_2 composite after charge-discharged for 5000 laps at the current density of 30 A/g, its capacitance is eventually stabilized at 93 F/g, which is far higher than that (57 F/g) of the pure MnO_2. Therefore, the Mn_3O_4/G/CB composite has a good application value as a supercapacitor electrode material.

ACKNOWLEDGEMENTS
This work is supported by the Natural Science Foundation of Shanxi (2014011017-2) and Scientific and Technological Innovation Programs of Higher Education Institutions in Shanxi (STIP, 2014113).

References

1. Y. Zhang, K. Y. Liu, W. Zhang, H. E. Wang, *Acta Chim. Sinica*, 66 (2008) 909.
2. K. T. Lee, C. B. Tsai, W. H. Ho, N. L. Wu, *Electrochem. Commun.*, 12 (2010) 886.
3. K. T. Lee, J. F. Lee, N. L. Wu, *Electrochim. Acta*, 54 (2009) 6148.
4. S. H. Li, Q. H. Liu, L. Qi, L. H. Lu, H. Y. Wang, *Chinese J. Anal. Chem.*, 40 (2012) 339.
5. F. Ran, H. Fan, L. Wang, L. Zhao, Y. Tan, X. Zhang, L. Kong, L. Kang, *J. Energy Chem.*, 22 (2013) 928.
6. X. Zhang, F. Ran, H. Fan, Y. Tan, L. Zhao, X. Li, L. Kong, L. Kang, *J. Energy Chem.*, 23 (2014) 82.
7. G. Zhu, L. Deng, J. Wang, L. Kang, Z. H. Liu, *Colloids Surf. A Physicochem. Eng. Asp.*, 434

(2013) 42.
8. H. Jiang, Y. Dai, Y. Hu, W. Chen, C. Li, *ACS Sustain Chem. Eng.*, 2014, 2: 70.
9. V. H. Nguyen, V. C. Tran, D. Kharismadewi, J. J. Shim, *Mater. Lett.*, 147 (2015) 123.
10. D. Ma, Z. Wu, Z. Cao, *J. Energy Chem.*, 23 (2014) 346.
11. R. Chandrasekaran, J. Palma, M. Anderson, *J. Energy Chem.*, 24 (2015) 264.
12. J. Duay, S. A. Sherrill, Z. Gui, E. Gillette, S. B. Lee, *Acs Nano.*, 7 (2013) 1200.
13. S. P. Yu, Q. Lu, R. T. Liu, K. F. Han, Z. M. Wang, H. Zhu, *Acta Chim. Sinica*, 70 (2012) 2359.
14. J. Hu, A. B. Yuan, Y. Q. Wang, X. L. Wang, *Acta Phys.-Chim. Sin.*, 25 (2009) 987.
15. J. Chang, M. Jin, F. Yao, T. H. Kim, V. T. Le, H. Yue, F. Gunes, B. Li, A. Ghosh, S. Xie, Y. H. Lee, *Adv. Funct. Mater.*, 23 (2013) 5074.
16. D. Kong, J. Luo, Y. Wang, W. Ren, T. Yu, Y. Luo, Y. Yang, C. Cheng, *Adv. Funct. Mater.*, 24 (2014) 3815.
17. S. L. Wang, J. B. Zhang, Z. H. Dong, B. Li, *Textile Auxiliaries*, 27 (2010) 24.
18. W. S. Hummers, R. E. Offeman, *J. Am. Chem. Soc.*, 80 (1958) 1339.
19. L. Lu, S. Xu, J. An, *Int. J. Electrochem. Sci.*, 11 (2016) 6287.
20. S. Yan, L. Gao, S. Zhang, W. Zhang, Y. Li, L. Gao, *Electrochim. Acta*, 94 (2013) 159.
21. S. Yan, L. Gao, S. Zhang, L. Gao, W. Zhang, Y. Li, *Int. J. Hydrogen Energy*, 38 (2013) 12838.
22. S. Yan, S. Zhang, W. Zhang, J. Li, L. Gao, Y. Yang, Y. Gao, *J. Phys. Chem. C*, 118 (2014) 29845.
23. X. Du, C. Zhou, H. Y. Liu, Y. W. Mai, *J. Power Sources*, 241 (2013) 460.
24. X. L. Li, G. Y. Zhang, X. D. Bai, X. M. Sun, X. R. Wang, E. Wang, H. J. Dai, *Nat. Nanotechnol.*, 3 (2008) 538.
25. J. H. Liu, J. W. An, Y. X. Ma, M. L. Li, R. B. Ma, *J. Electrochem. Soc.*, 159 (2012) A828.
26. J. An, J. Liu, Y. Ma, R. Li, M. Li, M. Yu, S. Li, Eur. Phys. *J. Appl. Phys.*, 58 (2012) 30403.
27. M. S. Wu, Z. S. Guo, J. J. Jow, *J. Phys. Chem. C*, 114 (2010) 21861.
28. Y. Y. Gao, S. L. Chen, D. X. Cao, G. L. Wang, J. L. Yin, *J. Power Sources*, 195 (2010) 1757.
29. J. Liu, J. An, Y. Zhou, Y. Ma, M. Li, M. Yu, S. Li, *Acs. Appl. Mater. Inter.*, 4 (2012) 2870.
30. L. L. Zhang, X. S. Zhao, *Chem. Soc. Rev.*, 38 (2009) 2520.
31. Q. F. Zhang, E. Uchaker, S. L. Candelaria, G. Z. Cao, *Chem. Soc. Rev.*, 42 (2013) 3127.
32. X. Wang, Y. Zhang, C. Zhi, X. Wang, D. Tang, Y. Xu, Q. Weng, X. Jiang, M. Mitome, D. Golberg, Y. Bando, *Nat. Commun.*, 4 (2013) 3905.